Low-cost, Continuously Variable, Strain Wave Transmission Using Gecko-inspired Adhesives

Nicholas D. Naclerio[1], Capella F. Kerst[2], David A. Haggerty[1], Srinivasan A. Suresh[2], Sonali Singh[2], Kenichi Ogawa[3], Susumu Miyazaki[3], Mark R. Cutkosky[2], and Elliot W. Hawkes[1]

***Abstract*—In robotics, high gear reductions are often required when using an electromagnetic motor to drive revolute joints, as in a humanoid robot. Strain wave gears (SWGs), also known as harmonic drives, are often used. However, these transmissions are relatively expensive and have a fixed gear ratio. Here we present a low-cost transmission that maintains the high reduction of the SWG and enables a continuously variable gear ratio. We achieve this by: (i) replacing the teeth of an SWG with a smooth frictional contact to enable continuous gear variation, and (ii) inverting the gear elements to enable high frictional torque transfer with a low preload via the capstan effect. We choose a gecko-inspired dry adhesive as the frictional material because it has high friction at low normal forces, and is not inherently tacky. We present a model describing the transmission, as well as experimental data gathered from a prototype device that verifies this model and establishes a proof of concept. Our transmission expands the possibilities for low cost robotic systems.**

***Index Terms*—Mechanism Design, Soft Robot Materials and Design, Power Transmission, Dry Adhesives.**

I. Introduction

MANY robotic applications use speed reducing transmissions to match high-speed electromagnetic motors to high torque outputs while maximizing efficiency. Matching motor capabilities to load requirements is particularly important for mobile robots, which often need to perform slow, high force movements, such as lifting objects [1].

One commonly used means of reduction in robotic applications is the strain wave gear (SWG), or harmonic drive. It is a compact device that can achieve gear reductions between 30:1 and 320:1 in a single stage [2]. This is significantly higher than simple planetary gears, which are limited to reductions of 10:1 per stage [3]. However, the SWG has limitations, particularly cost and a fixed gear ratio. The cost is a result of the tolerances required in the geometries of the meshing teeth and the diameters of the rotating parts – geometries that if not met reduce transmission efficiency and have the potential to destroy the gear's internal components [4]. The fixed gear ratio is a result of its reliance on intermeshing discrete teeth.

Because of the fixed gear ratio, SWGs are often used in series with transmissions that can change gear ratios, such as

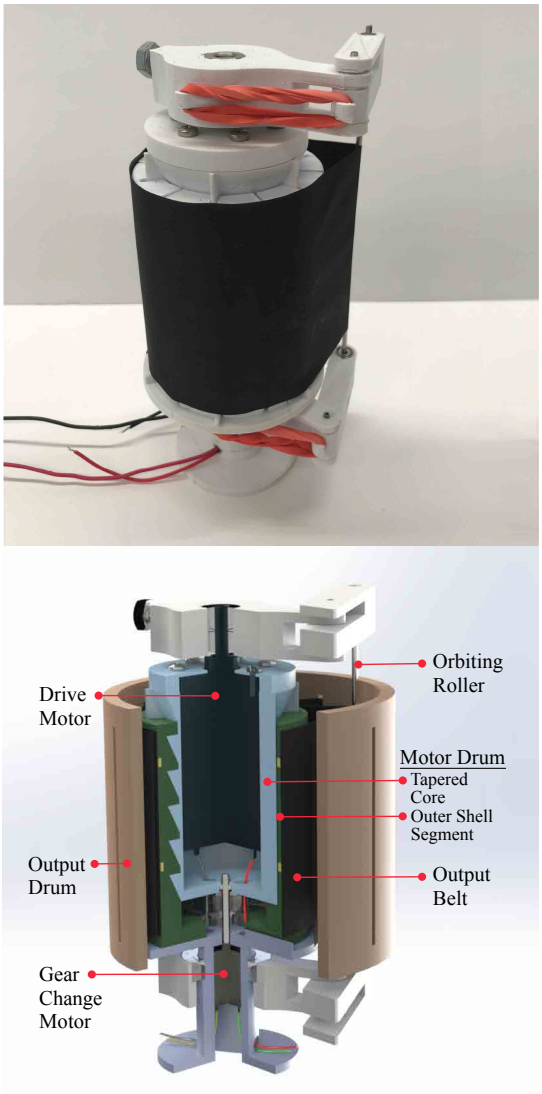

Fig. 1. The continuously variable strain wave gear (CVSWT). The motor input drives an orbiting roller that results in a slowly precessing output belt. The output drum is not shown in the photo. Prototype height is 15 cm.

Manuscript received: September, 10, 2018; Revised December, 14, 2018; Accepted January, 5, 2019.

This paper was recommended for publication by Paolo Rocco upon evaluation of the Associate Editor and Reviewers' comments. *(Corresponding author: Nicholas Naclerio)*

[1]Nicholas D. Naclerio, David A. Haggerty, and Elliot W. Hawkes are with the Department of Mechanical Engineering, University of California, Santa Barbara, CA 93106, USA nnaclerio@ucsb.edu; davidhaggerty@ucsb.edu; ewhawkes@ucsb.edu

[2] Capella F. Kerst, Srinavasan A. Suresh, Sonali Singh, and Mark R. Cutkosky are with the Department of Mechanical Engineering, Stanford University, Stanford, CA 94305, USA ckerst@stanford.edu; sasuresh@stanford.edu; sonalisi@stanford.edu; cutkosky@stanford.edu

[3]Kenichi Ogawa and Susumu Miyazaki are with Honda R&D Co., Ltd., Wako-shi, Saitama 351-0188, Japan kenichi_ogawa@n.f.rd.honda.co.jp; susumu_miyazaki@n.f.rd.honda.co.jp

Digital Object Identifier (DOI): see top of this page.

continuously variable transmissions (CVTs). CVTs of many different designs are used in applications from motor scooters to robots [5,6] Because they can change gear ratio continuously, CVTs allow input motors to run at their most efficient or most powerful operating point over a range of output speeds.

All CVTs rely on frictional contact to transmit torque. When using hard materials, as in CVTs for automobiles, this limitation requires high internal forces and increases weight and cost. When using soft materials, as in CVTs with rubber V-belts, there are hysteretic and frictional losses.

The contribution of this paper is to address these limitations of conventional robotic transmissions using two key principles. First, we remove the teeth of the SWG and replace them with a smooth frictional contact; hence, a small change in diameter can be created without requiring a discrete change in the number of teeth. Second, we invert the gearing elements of a standard SWG to exploit the capstan effect. Working in combination with dry adhesives, this novel morphology enables high torque transfer with a very low preload.

Accordingly, we present a low-cost, 3-D printed continuously variable strain wave transmission (CVSWT), shown in figures 1, 5, and the accompanying video. Notably, it achieves the high reduction of an SWG while being continuously variable. Thus the common task in robotics of a large reduction with variable gear ratio can be implemented in a single transmission. Our design joins other drives that exploit creative geometries and materials, including a magnetic SWG [7], a fixed planetary gearing design that replaces toothed gears with compressed metal rollers [8], a variable planetary gearing drive with smooth conical rollers [9], systems with orbiting pulleys [10], and a variable transmission using high tension (1 kN to 3 kN) nested pulleys [11]. This paper describes our design, analytic modeling, fabrication, and testing of a proof-of-concept prototype.

II. Principles of a Continuously Variable Strain Wave Transmission

In this section, we describe the operation of a standard SWG, then we describe two principles that allow us to create a CVSWT. First, we replace teeth with smooth frictional surfaces to allow continuous variation. Second, we invert the gearing elements to leverage the capstan effect and enable high torque transfer using friction without a high preload.

Standard SWG Operation: A standard SWG consists of a fixed outer spline, a flexible inner spline (flexspline), and an elliptical wave generator in the center (Fig. 2, left). The circumference of the flexspline is chosen to be slightly smaller than the fixed spline by an integer number of teeth. The wave generator forces the flexspline to mesh with the outer spline at two points. For every rotation of the wave generator, the flexspline precesses in the opposite direction by the difference in its perimeter and that of the outer spline. For example, given a fixed spline and a flexspline with 202 and 200 teeth respectively, every rotation of the wave generator causes the flexspline to rotate in the opposite direction by 2 teeth; a gear reduction of 100:1. Continuous variation is not possible because of the discrete teeth; if the number of teeth on the flexspline or fixed ring changed, it would result in large jumps in gear ratios.

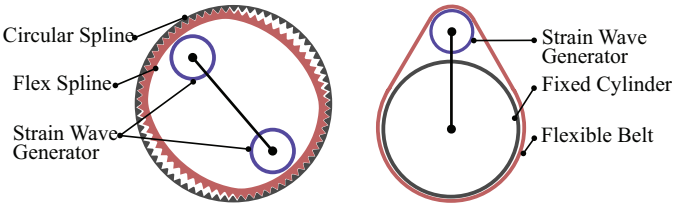

Fig. 2. Left: illustration of the gearing element of a standard SWG. Right: illustration of the gearing elements of the CVSWT. The two principles shown here are: (i) smooth contacting surfaces to allow continuous variation, and (ii) an inverted morphology to allow high torque transfer with low preload through capstan friction.

Principle 1: Smooth Frictional Contacts: To address the challenge of continuous variation, the first principle of the CVSWT is to replace discrete toothed contacts with smooth frictional contacts[1]. As such, the gear ratio can be varied continuously by slightly changing the relative sizes of the gear elements. While a standard SWG relies on mechanical interlocking to transmit torque, a friction-based design with a standard SWG morphology would require a very large preload force to transmit high torque. This is feasible in a fixed-gearing scenario, but impractical in a low cost, continuously variable case.

Principle 2: Inversion of Gearing Elements: To create high friction without a large normal preload, the gearing elements are inverted in the CVSWT to exploit the capstan effect [13,14]. Rather than place the flexible element inside the fixed component, the fixed component is wrapped with a flexible belt of a slightly larger diameter. This leaves some slack in the belt, which is kept at a single point (rather than the two points in a standard SWG) to maximize the wrap angle of the belt around the drum, maximizing the capstan effect. A wave generating mechanism forces this slack around the circumference of the fixed cylinder. If there is no slip between the contacting portions of the belt and the fixed cylinder, then the belt will rotate by the difference in circumference of the two elements, in a manner analogous to the standard SWG. As in an SWG, the wave generator acts as input, and the flexible element as the output.

These two principles—(i) replacing teeth with smooth frictional surfaces to allow continuous variation, and (ii) inverting the gearing elements to enable high torque transfer through friction without a high preload—allow a low-cost CVSWT.

III. Design

We now consider the specific design decisions made to create our prototype CVSWT.

A. Variable Circumference Motor Drum

Continuous gear ratio variation requires changing the relative size of gearing elements. We vary the diameter of the fixed cylinder, which houses the drive motor and is referred to as the motor drum. The drum consists of four components: a

[1]Interestingly, Musser's original SWG patent mentions that its fundamental function will not change by replacing teeth with friction contacts [12].

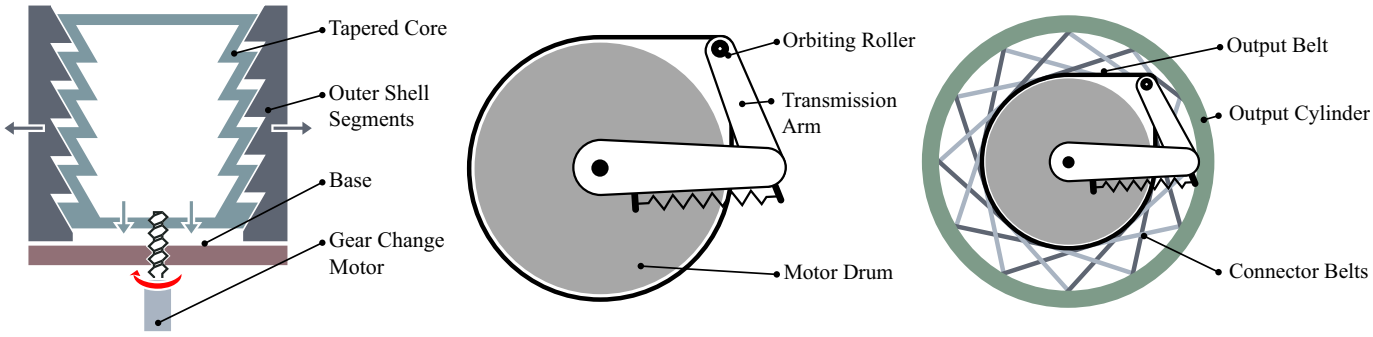

Fig. 3. Illustration of the basic CVSWT components from left to right: variable circumference motor drum, orbiting roller and transmission arm, and output cylinder.

tapered core that contains the drive motor, an outer shell with a matching taper that is cut radially into six segments and compressed by hoop springs, a base constraining the core and shell to each other, and an actuator to change the diameter (Fig. 3). Ridges along the length of the tapered core mate with grooves in the outer shell segments to transmit torque. As the core moves towards the base, the outer shell segments are pushed radially outward by the taper, increasing the motor drum diameter. Conversely, as the tapered core moves upward, the spring around the shell segments returns them to their original position. To increase stability and increase the available space within the motor drum, the tapered core is split into a series of conical segments. An actuator with a leadscrew moves the core with respect to the base.

B. Orbiting Roller

As described in Sec. II, there must be a wave generator to move the belt slack around the drum. This is accomplished with an orbiting roller (Fig. 3). Its ends are attached to the transmission by two arms: one to the output shaft of the drive motor, and one to the base of the drum. The arms are hinged at their centers to allow the roller to maintain tension on the belt as the drum diameter changes. These joints are biased outwards with springs, and configured so that joint torque is approximately constant over the small angular deflection of the links. A small counter-weight is attached on the arm opposite the roller to improve rotational stability.

C. Gecko-inspired Dry Adhesive

To create high friction between the motor drum and output belt, we apply a gecko-inspired dry adhesive to the drum, and use a thermoplastic urethane (TPU) coated nylon fabric belt. The dry adhesive has both high adhesion-controlled friction and a high coefficient of friction [15]. Adhesion-controlled friction is a frictional force that is caused by an adhesive force [16]. This differs from the more familiar load-controlled friction, which is a frictional force caused by an applied normal load. The combination of high adhesion-controlled and load-controlled friction means that even at very low belt tension, the dry adhesive generates high friction, and therefore allows large output torques.

Our specific dry adhesive was chosen because it is not inherently tacky; it only generates strong adhesion when loaded in shear, and can engage and disengage rapidly [15]. This switching is fast, due to the microstructure of the adhesive material, requiring less than 75 ms [17]. Together, these properties of controlled and rapid adhesion allow it to be used with relatively high efficiency in a transmission (Sec. VI-C), where it must undergo a high loading cycle rate without imposing large hysteretic effects.

D. Output Cylinder

We connect a rigid output cylinder to the output belt of the CVSWT to provide a well-constrained output. This differs from an SWG, which attaches a flexible cup output to the flexspline. With our selected design and materials, the flex cup is impractical because of the torsional buckling of the belt. The output cylinder is attached to the output belt by 24 connector belts. Each belt is attached at one end to the output drum, and at the other end tangentially to the output belt (Fig. 3). 12 belts are wrapped clockwise, and the other 12 counterclockwise to prevent backlash. The belts are tensioned such that torque is transferred from the output belt to the output drum, while still allowing radial movement of the output belt to accommodate the orbiting roller.

IV. Modeling

Here we present mathematical models of the CVSWT that describe its gear ratio and maximum expected torque as functions of relevant design parameters.

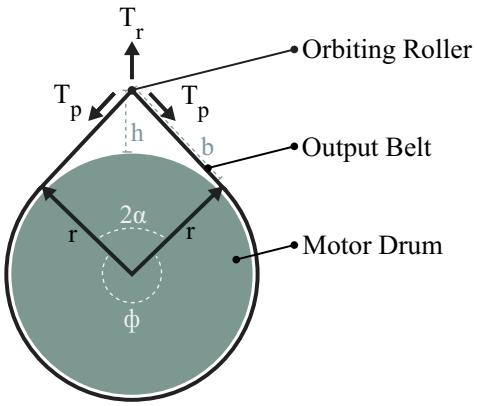

Fig. 4. Illustration of transmission geometry for use in modeling.

A. Gear Ratio

The gear reduction of the CVSWT is dependent only on the circumference of the motor drum relative to the length of the output belt. The gear reduction for a traditional SWG with a fixed circular spline and output flexspline can be written as:

$$\text{Reduction} = \frac{N_{\text{flex}}}{N_{\text{flex}} - N_{\text{circ}}}. \tag{1}$$

where N_{flex} and N_{circ} are the number of teeth on the flexspline and circular spline respectively. Replacing these terms with their analogues in our transmission, the equation becomes

$$\text{Reduction} = \frac{L_{\text{belt}}}{L_{\text{belt}} - L_{\text{drum}}}, \tag{2}$$

where L_{belt} and L_{drum} are the length of the belt and the circumference of the drum respectively. Notably, the gear reduction is no longer constrained by a discrete number of teeth, and can be changed by altering either L_{belt} or L_{drum}. We vary L_{drum} in the presented design.

B. Maximum Torque

The maximum torque that the CVSWT can transmit is dependent on the friction between the motor drum and output belt, as well as the current gear ratio. The gear ratio affects the maximum torque because as the drum shrinks in size, the belt is in contact with the drum over a smaller area and wrap angle.

1) Dry Adhesive Capstan Equation Derivation: The maximum torque can be found by deriving the capstan equation [13] with negligible bending stiffness, and including an adhesive friction component provided by the dry adhesive. Given a belt wrapped over a drum with a contact angle ϕ, and belt tensions T_{hold} and T_{load}, we consider a segment of belt contacting over a differential angle $\mathrm{d}\theta$. This belt has tensions T and $T+\mathrm{d}T$ at either end. Summing radial forces around the center of the belt element, we have

$$\mathrm{d}F_{\text{n}} - T\frac{\mathrm{d}\theta}{2} - (T+\mathrm{d}T)\frac{\mathrm{d}\theta}{2} = 0, \tag{3}$$

where $\mathrm{d}F_{\text{n}}$ is the normal force on the belt, and we have made the small-angle approximation to simplify sines. Ignoring the higher-order term, we obtain

$$\mathrm{d}F_{\text{n}} = T\mathrm{d}\theta. \tag{4}$$

We model the friction force, F_{s}, between two surfaces as

$$F_{\text{s}} = A\sigma_0 + \mu F_{\text{n}}, \tag{5}$$

where A is the contact area, σ_0 is an adhesion-controlled friction stress, and μ is a constant relating additional normal force to additional friction force [16]. When σ_0 is negligible, this is the conventional coefficient of friction.

The change in tension $\mathrm{d}T$ over a wrap angle $\mathrm{d}\theta$ is the frictional force over that infinitesimal length. Combining equations 4 and 5, and writing $\mathrm{d}A$ as $wr\,\mathrm{d}\theta$ where w is the belt width, and r is the drum radius:

$$\begin{aligned}\mathrm{d}T &= \mathrm{d}F_{\text{s}} \\ &= \mathrm{d}A\sigma_0 + \mu\mathrm{d}F_{\text{n}} \\ &= wr\sigma_0\,\mathrm{d}\theta + \mu T\mathrm{d}\theta \\ &= (wr\sigma_0 + \mu T)\,\mathrm{d}\theta,\end{aligned} \tag{6}$$

which has a solution

$$T(\theta) = Ce^{\mu\theta} - \frac{wr\sigma_0}{\mu}. \tag{7}$$

Substituting $\theta = 0$, $T(0)$ is by definition T_{hold}, and we can solve for C:

$$C = T_{\text{hold}} + \frac{wr\sigma_0}{\mu}. \tag{8}$$

Evaluating at $\theta = \phi$, the tension is equal to T_{load}, and we obtain the modified capstan equation for a dry adhesive:

$$T_{\text{load}} = \left(T_{\text{hold}} + \frac{wr\sigma_0}{\mu}\right)e^{\mu\phi} - \frac{wr\sigma_0}{\mu}. \tag{9}$$

2) Torque: T_{hold} can be found from a known radial force provided by the orbiting roller. Assuming that this force is balanced by tension in the two sides of the belt, the force balance is

$$T_{\text{r}} = 2T_{\text{p}}\sin(\alpha), \tag{10}$$

where T_{r} is the tension applied by the orbiting roller, T_{p} is the pre-load tension on the belt and assumed to be the only tension contributing to T_{hold}, and 2α is the angle swept by the drum surface not in contact with the belt (Fig. 4). Solving for T_{hold}, eq. 10 becomes

$$T_{\text{hold}} = T_{\text{p}} = \frac{T_{\text{r}}}{2\sin(\alpha)}. \tag{11}$$

The maximum torque that the transmission can handle, τ_{max}, is simply $T_{\text{load}} \cdot r$. From equations 9 and 11, τ_{max} can be written as

$$\tau_{\text{max}} = T_{\text{load}} \cdot r = \left[\left(\frac{T_{\text{r}}}{2\sin(\alpha)} + \frac{wr\sigma_0}{\mu}\right)e^{\mu\phi} - \frac{wr\sigma_0}{\mu}\right] \cdot r. \tag{12}$$

3) Finite Surface Area Drum: Because the presented device changes motor drum size using a finite number of outer shell segments expanding radially outward, eq. 12 is not entirely accurate. As the drum expands, its surface area does not actually increase. Compensating for this effect by scaling the contacted area as a fraction of the drum surface area, eq. 12 becomes

$$\tau_{\text{max}} = \left[\left(\frac{T_{\text{r}}}{2\sin(\alpha)} + \frac{wr_0\sigma_0}{\mu}\right)e^{\mu\phi} - \frac{wr_0\sigma_0}{\mu}\right] \cdot r, \tag{13}$$

where r_0 is the drum radius at its minimum size.

C. Belt Contact Angle as a Function of Gear Ratio

To determine the maximum torque from eq. 13 as a function of gear ratio, we must write the wrap angle, ϕ, as a function of the gear ratio, or equivalently, motor drum size (a change in gear ratio changes the diameter of the motor drum and thus wrap angle). As can be seen in Fig. 4, ϕ can be written in terms of α as

$$\phi = 2\pi - 2\alpha, \tag{14}$$

where α is half of the arc angle not in contact with the belt. If the orbiting roller's diameter is much less than that of the drum, its effect on belt shape is negligible and α can be written in terms of b and r as

$$\alpha = \arctan\frac{b}{r}, \tag{15}$$

Fig. 5. CVSWT prototype with arm attached to the output drum. The CVSWT is mounted parallel to the ground, such that through the CVSWT, the drive motor can rotate the arm and lift a 1 kg water bottle, exerting 2.5 N·m of torque (see accompanying video).

where b is the length of one side of belt not in contact with the drum. Writing an expression for the full belt length, we get

$$L_{\text{belt}} = L_{\text{drum}} + 2(b - r\alpha). \tag{16}$$

The system of equations 14, 15 and 16 can be solved numerically to find ϕ in terms of r, giving the belt wrap angle for a given gear ratio.

V. Prototype Fabrication

One advantage of the CVSWT is that because of its unique design and low belt tension, it can be made with inexpensive materials and low tolerances. A proof-of-concept prototype was built, and can be seen in figures 1 and 5. All plastic parts were 3D printed in polylactic acid themoplastic (PLA) on a Lulzbot Taz 6 with a 0.38 mm layer height and 20% fill density. Any imperfections were cut off or filed down during assembly.

A. Variable Circumference Motor Drum

The motor drum as described in Sec. III-A and Fig. 3 houses a 37 mm, 12 V DC drive motor. The drum components (the tapered core, the six outer shell pieces, and the base) are all made of PLA. The inward bias force on the shell segments is provided by two rubber bands wrapped around their circumference. A micro metal DC gear motor with a threaded rod connected to a nut fixed to the bottom of the tapered core drives the diameter changes. The motor is non-backdrivable to maintain a constant gear ratio.

B. Orbiting Roller

The orbiting roller is made of a 3.2 mm diameter hardened stainless steel rod connected on each end to PLA tensioner arms as described in Sec. III-B. One arm is fixed to the drive motor with a shaft coupler, and the other is free to rotate on a bearing around the base of the CVSWT. Short 2 mm diameter steel rods form the hinge joints of the arms, and rubber bands bias them outward. An M6 steel screw attached to the base of each arm, opposite the roller, acts as a counterweight.

C. Gecko-Inspired Dry Adhesive

The dry adhesive was cast in silicone (Dragon Skin 30, Smooth-On), using a micromachined mold as in [18]. 0.5 mm thick strips are bonded to the outer face of the shell segments of the motor drum using a room temperature vulcanizing silicone adhesive (Sil-Poxy, Smooth-On), covering 40 mm in height. Prior work has shown that the dry adhesive will retain about 70% of its adhesiveness without cleaning over 3×10^4 attachment and detachment cycles [19].

D. Output Cylinder

The output cylinder described in Sec. III-D is made of PLA, and the output belt and connector belts are made of a 0.2 mm thick, TPU coated, 70 Denier rip-stop nylon (Seattle Fabrics) with a tensile strength of 660 N/5cm [20]. To simplify construction, only clockwise orientated belts were used in the prototype (Fig. 5). This limits effective torque transfer to clockwise rotations. The belts are formed from strips of fabric, with one end heat sealed to the output belt, and the other adhered to the drum with double-sided tape (Red-e Tape, TrueTape). The lifespan of the belt remains to be determined, however in other flat belt drive applications the belts can last for years when slippage is kept low [21]. A simple robot arm was attached to the output drum to demonstrate a potential application of the CVSWT (Fig. 5 and accompanying video). Note that the output cylinder vibrates slightly because it is fixed directly to the output belt. This effect could be eliminated with a flex cup, as in a traditional SWG.

E. Size, Weight and Cost

The CVSWT prototype is 15 cm in height, and 10 cm in diameter. It has a mass of 520 g. Without the drive motor and gear change motor its mass is 280 g.

The material costs of the prototype are approximately 47 USD. This value does not include the motors because they are not inherent to the CVSWT. The majority of the cost is from 42 USD in bearings, while the dry adhesive silicone costs only 0.15 USD. Hardware and bearing costs are taken from item prices listed by McMaster-Carr, PLA cost is based on the cost per weight of eSUN PLA Pro+, and the dry adhesive cost is based on the cost per weight of Dragon Skin 30 (Smooth-On).

VI. Results

We present experimental results that validate the models from Sec. IV, and describe the efficiency of the dry adhesive during torque transfer, as well as the overall CVSWT efficiency.

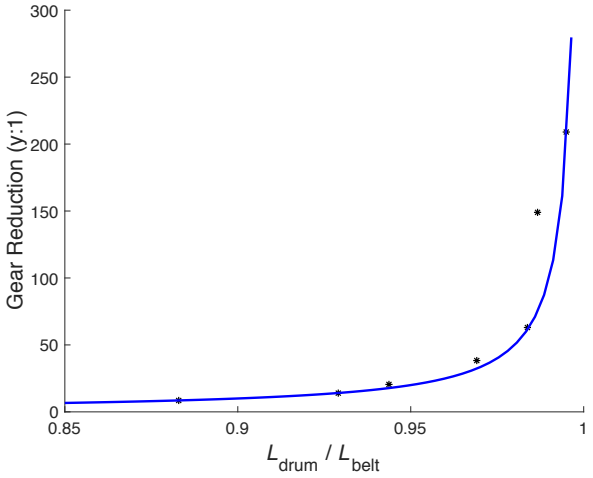

Fig. 6. Measured gear reductions plotted as points with respect to the ratio of drum circumference (L_{drum}) over belt length (L_{belt}). Theoretical values from eq. 2 are plotted as a blue line.

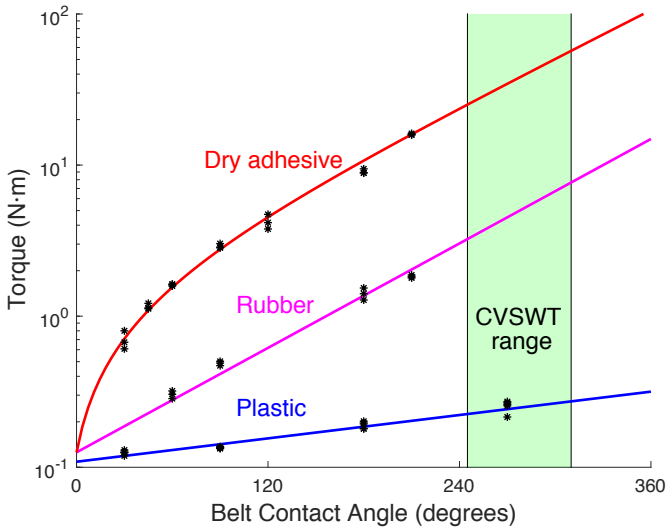

Fig. 7. Results showing maximum torque before belt slip as a function of wrap angle on plastic, rubber, and dry adhesive (black points). Theoretical values from eq. 13 are plotted as lines using fitted μ and σ_0 values (see Sec. VI-B). The green box represents the range of belt angles that the CVSWT can operate in. The segment of the red, dry adhesive fit line in this box indicates the theoretical maximum torque that the CVSWT can transmit.

A. Gear Ratio

To confirm eq. 2, the gear reduction of the transmission was measured at a range of drum diameters from 60 mm to 68 mm. This was done by observing the number of times that a 2 mm orbiting roller cycled per the number of times the flexible belt (without the outer cylinder) completed a rotation at a given motor drum size. The transmission was observed until the belt made a complete rotation, or the number of roller cycles exceeded 60, whichever involved more cycles. The drum diameter was recorded as the average of three different measurements with calipers. The measurements varied slightly ($\pm$0.5 mm) because the outer shell of the motor drum is made up of six separate segments. The length of the belt was measured to be 214.5 mm.

The measured gear ratios of the CVSWT, as a function of the motor drum circumference divided by the belt length, are shown in Fig. 6 along with their theoretical values from eq. 2, verifying the model. Measured gear ratios ranged from 8.5:1 to 209:1, a change of 24.6$\times$. Note that the gear ratio increases exponentially as the drum circumference approaches the belt length. This effect could be mitigated by remaining in lower gear ratios, such as between 8.5:1 and 85:1, which still provide a 10$\times$ gear change.

B. Maximum Torque of Dry Adhesive and Flexible Belt

We tested the maximum torque that could be transmitted between the motor drum and flexible belt as a function of wrap angle with three drum surfaces: PLA, high-friction rubber without measurable adhesion, and dry adhesive. This was done by measuring the tangential force required to slip the belt at various wrap angles.

For all tests we positioned the 62 mm diameter motor drum horizontally and draped a 40 mm wide strip of flexible belt fabric, reinforced with ballistic nylon, over it. From one end hung a weight that delivered a constant pre-tension of 4 N, and on the other end was attached a force sensor (M3-5 or M3-100, Mark-10). 3-5 trials each were conducted at various wrap angles from 30° to 270°, measuring the belt tension required to slip the belt. Measurements with the dry adhesive were limited to 210° and 16 N·m because they exceeded the 500 N rating of our Mark-10 M3-100 force sensor.

Data are shown in Fig. 7, along with the model predictions from eq. 13. We use fitted parameters, with μ of 0.18 and σ_a of 0 kPa for PLA, μ of 0.76 and σ_a of 0 kPa for rubber, and μ of 0.7 and σ_a of 29 kPa for the dry adhesive. The values for the adhesive are consistent with testing on flat surfaces, supporting eq. 13.

The shaded region in Fig. 7 covers the actual range of belt contact angles experienced by the CVSWT over its full range of gear ratios, from 245° to 350° (found by numerically solving equations 14, 15, and 16). Torque fit line segments that fall in this region are therefore the theoretical maximum values of the CVSWT. This suggests that the theoretical maximum torque that the CVSWT can transmit with only a 4 N belt tension ranges from 25 N·m to 57 N·m, depending on gear ratio. This could be increased with higher belt tension.

Because we were limited by our sensor force capacity, we did not test past 210° with the dry adhesive. Note that these tests are at constant preload belt tensions. The actual CVSWT has a relatively constant orbiting roller tension (T_r from 3.34 N to 3.84 N), so from eq. 13 this would cause the belt pre-load (T_p), and in turn maximum torque, to increase exponentially as α decreases at higher gear ratios. This effect is not represented in Fig. 7.

This test suggests that even at a low pretension of 4 N, at the belt wrap angles in the CVSWT, the belt will not slip at 25 N·m. Under a high torque, other components of the CVSWT would likely fail before friction between the drum and the belt is overcome, making slight changes in adhesion due to temperature or humidity inconsequential.

TABLE I
BELT/ROLLER MATERIALS AND EFFICIENCIES

Materials	Speed	Stainless Glass	TPU Fabric Glass	TPU Fabric Dry Adhesive
Efficiency, η_B	250 rpm	0.979	0.976	0.947
	1000 rpm	0.947	0.976	0.933

C. Torque Transfer Efficiency Test Using Dry Adhesive

A simplified dynamometer apparatus was constructed to measure the efficiency of transferring torque through dry adhesives and a belt. The expected contributions to power loss in such a configuration are slippage (speed loss) and rolling resistance between the belt and drum (torque loss) [22].

The apparatus consists of two 47 mm diameter rollers of glass tubing with aluminum end caps that rotate on low friction precision ball bearings. The input torque is supplied by a motor (Maxon RE35-118776) to the input roller. The output roller is attached to an electromagnetic hysteresis brake (Magtrol HB-38-2). Encoders (EM1-2-500-N, US Digital) measure the speeds at the input and output rollers.

The configuration was tested with three different combinations: (i) a TPU-coated nylon fabric belt as described in Sec. V-D with dry adhesive film covering the rollers, (ii) the same belt without dry adhesive on the rollers, and (iii) a 0.1 mm thick stainless steel belt without adhesive on the rollers to approximate conditions using conventional hard materials. The motor and input roller assembly were characterized to provide a known input torque for various combinations of supplied current and speed. The output torque was supplied by the electromagnetic brake, which was similarly characterized.

Table I shows that efficiencies for all three combinations are high, as expected for thin belts on smooth rollers [23]–[25]. For the stainless steel on glass and TPU-coated fabric on glass cases, the energy loss is due to small amounts of slippage; rolling resistance is negligible. Conversely, for the TPU coated fabric on adhesive clad rollers, the slippage is negligible (despite using a much lower belt tension than for the steel belt) but there is a small amount of rolling resistance between the belt and the rollers. This result suggests that a transmission using a fabric belt and dry adhesives could be efficient, comparing favorably to conventional transmissions with gears or SWGs.

D. Overall CVSWT Efficiency

The overall efficiency of the CVSWT was determined as the ratio of transmission output power to input power over a range of gear ratios while lifting a mass. The CVSWT was positioned upright, as in Fig. 1, with two light Spectra cables wrapped around the output cylinder, running over low friction pulleys and attached to variable masses. Three trials were taken at each tested gear ratio. Motor input power was measured as I·V from an Eventek KPS3010D DC power supply to the drive motor. For each test, motor input power was held roughly constant at about 3 W by keeping voltage at a constant 6 V and varying the masses by 0.5 kg increments to keep the average current close to 0.5 A. The resultant torque on the transmission ranged from 0.5 N·m to 2.5 N·m. The average current was calculated as the average of six current readings. Output power was measured as mgv where m is the weight of the variable mass, g is the gravitational constant, and v is the velocity that the mass rises at, measured as the height to the closest cm it rose over 20 s.

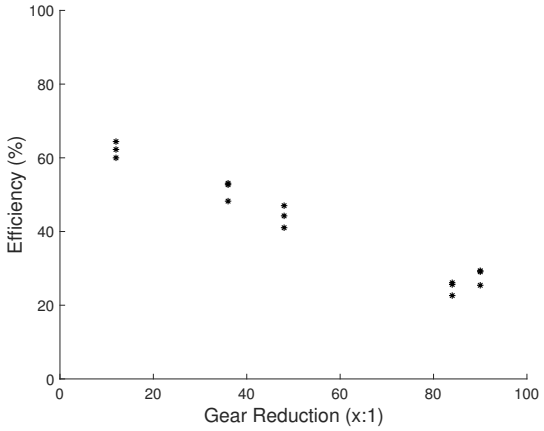

Fig. 8. Experimental CVSWT efficiency measurements at various gear ratios.

The efficiency of the drive motor (η_M) was characterized in a similar way, by recording input power while lifting various masses without the CVSWT at a constant voltage of 6.0 V and with current from 0.45 A to 0.55 A to match the motor input power range tested with the CVSWT. The motor efficiencies are fairly constant in this range, so a linear fit of the experimental data was used to supply η_M. The overall transmission efficiency is therefore

$$\eta_T = \frac{P_{out}}{P_{in}} = \frac{mgv}{IV\eta_M} \tag{17}$$

where η_T and η_M are the CVSWT and drive motor efficiencies respectively. η_T is dependent on input power and gear ratio, and η_M is dependent on input power.

The efficiency of the prototype is presented in Fig. 8 and ranges from 23% at 84:1 to 64% at 12:1. It is inversely proportional to the gear reduction, which suggests that it is directly proportional to the rate at which the orbiting roller spins relative to the output drum. These efficiencies are much lower than those in Table I, however the prototype was built as a proof-of-concept of simple construction, without optimizing for maximum efficiency, high power transmission, or stiffness (the output stiffness of the device, when under load, is 51 N·m/rad).

VII. DISCUSSION

The goal of this work was to create a light and inexpensive SWG with the ability to continuously change gear ratios. We met these goals with our 3D printed proof-of-concept prototype CVSWT, capable of changing gear ratios from 8.5:1 to 209:1, a change of 24.6×. For comparison, most automobile CVTs vary their gear ratio by 6× [26]. Critical in enabling these characteristics are the two presented principles: (i) a smooth torque transfer interface with a dry adhesive that allows continuous gear ratio variation, and (ii) an inversion

of the gearing elements that allows the use of the capstan effect for high torque transfer.

Surprisingly, the use of the dry adhesive resulted in only a small reduction in efficiency (a few percent). This is likely because the adhesive is not inherently tacky, meaning there is no peeling required to remove the belt from the drum during rotation. The overall efficiency of the CVSWT prototype however is lower, but still reasonable for a simply constructed proof-of-concept.

Importantly, torque is not limited by belt slippage. This is a result of combining the capstan effect with the high friction dry adhesive. We showed a theoretical peak torque transfer before belt slip of over 57 N·m at the highest gear ratio (Fig. 7). Notably, this far exceeds the result with high friction rubber, which has a higher coefficient of friction but no measurable adhesion. This points to the importance of using a dry adhesive because its adhesion-controlled friction significantly increases the maximum torque, as shown by this term multiplying the exponential in eq. 13. This allows the CVSWT to operate with low belt tension.

As with any design, there are tradeoffs with using compliant components in the CVSWT. Because of its flexible elements, the CVSWT will naturally have some imprecision in gear ratios and angular position. This makes the CVSWT unsuitable for tasks that require high positional accuracy, such as in pick and place robots. However, with angle encoders on the transmission input and output, a feedback control loop could be used to reliably control position and gear ratio. Further, the CVSWT is better suited for low cost, low weight applications that do not depend on a high degree of positional accuracy or stiffness, such as in hospital and household assistance robots [27,28].

VIII. Conclusion

In this paper we have presented a novel design of a transmission that uses a smooth torque transfer surface and an inverted morphology compared to a standard SWG. We use a gecko-inspired dry adhesive to enhance friction at the torque transfer surface and show a low cost, continuously variable, strain wave transmission with high gear reductions and torque rating. Further work would involve optimizing the design and packaging to make it more compact and robust. This CVSWT could be used in robots that require both a high gear reduction and a variable transmission at low cost.

Acknowledgment

S.A. Suresh is supported by a NASA Space Technology Research Fellowship.

References

[1] K. Kaneko, K. Harada, F. Kanehiro, G. Miyamori, and K. Akachi, "Humanoid robot hrp-3," in *IEEE/RSJ Int. Conf. Intelligent Robots and Systems*, 2008, pp. 2471–2478.

[2] K. Ueura and R. Slatter, "Development of the harmonic drive gear for space applications," in *Proc. 8th European Symp. Space Mechanisms and Tribology*, vol. 438. ESA SP Publ., 1999, pp. 259–264.

[3] A. Pantelides and G. Antony, "Precision planetary servo gearheads," American Gear Manufacturers Association, Tech. Rep. 06FTM04, 2006.

[4] H. Dong, D. Wang, and K.-L. Ting, "Kinematic effect of the compliant cup in harmonic drives," *J. Mech. Design*, vol. 133, no. 5, p. 051004, 2011.

[5] N. Srivastava and I. Haque, "A review on belt and chain continuously variable transmissions (cvt): Dynamics and control," *Mech. Mach. Theory*, vol. 44, no. 1, pp. 19–41, 2009.

[6] M. A. Kluger and D. R. Fussner, "An overview of current cvt mechanisms, forces and efficiencies," SAE Technical Paper, Tech. Rep., 1997.

[7] J. Rens, K. Atallah, S. D. Calverley, and D. Howe, "A novel magnetic harmonic gear," *IEEE Trans. Industry Applications*, vol. 46, no. 1, pp. 206–212, 2010.

[8] J. F. Schorsch, "Compound planetary friction drive," U.S. Patent App. 15/461,170, 6 29, 2017.

[9] C. Everarts, B. Dehez, and R. Ronsse, "Novel infinitely variable transmission allowing efficient transmission ratio variations at rest," *Hip*, vol. 200, p. 250, 2015.

[10] O. Palma-Marrufo and C. A. Cruz-Villar, "Infinitely variable transmission kynematic design with orbital pulleys," in *IEEE Int. Conf. Electrical Engineering Computing Science and Automatic Control*, 2011, pp. 1–6.

[11] A. S. Kembaum, M. Kitchell, and M. Crittenden, "An ultra-compact infinitely variable transmission for robotics," in *IEEE Int. Conf. Robotics and Automation*, 2017, pp. 1800–1807.

[12] C. W. Musser, "Strain wave gearing," U.S. Patent 2,906,143, 9 29, 1959.

[13] J. H. Jung, N. Pan, and T. J. Kang, "Capstan equation including bending rigidity and non-linear frictional behavior," *Mech. Mach. Theory*, vol. 43, no. 6, pp. 661–675, 2008.

[14] H. In, S. Kang, and K.-J. Cho, "Capstan brake: Passive brake for tendon-driven mechanism," in *IEEE/RSJ Int. Conf. Intelligent Robots and Systems*, 2012, pp. 2301–2306.

[15] E. W. Hawkes, D. L. Christensen, A. K. Han, H. Jiang, and M. R. Cutkosky, "Grasping without squeezing: Shear adhesion gripper with fibrillar thin film," in *IEEE Int. Conf. Robotics and Automation*, 2015, pp. 2305–2312.

[16] J. N. Israelachvili, *Intermolecular and Surface Forces*, 2nd ed. Academic Press, 2015.

[17] D. L. Christensen, E. W. Hawkes, S. A. Suresh, K. Ladenheim, and M. R. Cutkosky, "μtugs: Enabling microrobots to deliver macro forces with controllable adhesives," in *IEEE Int. Conf. Robotics and Automation*, 2015, pp. 4048–4055.

[18] P. Day, E. V. Eason, N. Esparza, D. Christensen, and M. Cutkosky, "Microwedge machining for the manufacture of directional dry adhesives," *J. Micro. Nano-Manuf.*, vol. 1, no. 1, p. 011001, 2013.

[19] A. Parness, D. Soto, N. Esparza, N. Gravish, M. Wilkinson, K. Autumn, and M. Cutkosky, "A microfabricated wedge-shaped adhesive array displaying gecko-like dynamic adhesion, directionality and long lifetime," *J. R. Soc. Interface*, pp. 1223–1232, 2009.

[20] B. International. (2006) Data sheet for: Brook ripstop nylon fr. [Online]. Available: http://www.utilgraph.it/images/prodotti/schede/brook/Ripstop_Nylon_FR_V4.pdf

[21] T. Childs, K. Dalgarno, A. J. Day, and R. Moore, "Automotive timing belt life laws and a user design guide," *P. I. Mech. Eng. D-J. Aut.*, vol. 212, no. 5, pp. 409–419, 1998.

[22] W. Grzegożek and A. Kot, "The experimental analysis of the slip in the rubber belt cvt," in *IOP Conf. Series: Materials Science and Engineering*, vol. 148, no. 1, 2016, p. 012006.

[23] L. Kong and R. G. Parker, "Microslip friction in flat belt drives," *P. I. Mech. Eng. C-J. Mec.*, vol. 219, no. 10, pp. 1097–1106, 2005.

[24] T. Childs, "The contact and friction between flat belts and pulleys," *Int. J. Mech. Sci.*, vol. 22, no. 2, pp. 117–126, 1980.

[25] A. De Almeida and S. Greenberg, "Technology assessment: energy-efficient belt transmissions," *Energ. Buildings*, vol. 22, no. 3, pp. 245–253, 1995.

[26] Nissan. (2018) The xtronic continuously variable transmission. [Online]. Available: https://www.nissanusa.com/experience-nissan/news-and-events/xtronic-cvt-continuously-variable-transmission.html

[27] T. L. Chen and C. C. Kemp, "Lead me by the hand: Evaluation of a direct physical interface for nursing assistant robots," in *ACM/IEEE Int. Conf. Human-Robot Interaction*, 2010, pp. 367–374.

[28] M. Ciocarlie, K. Hsiao, E. G. Jones, S. Chitta, R. B. Rusu, and I. A. Şucan, "Towards reliable grasping and manipulation in household environments," *Spr. Tra. Adv. Robot.*, pp. 241–252, 2014.